Heliyon 10 (2024) e26584

Contents lists available at ScienceDirect

Heliyon

journal homepage: www.cell.com/heliyon

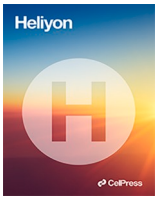

Research article

Seismic sedimentology response characteristics of nearshore terminal fan in the suning area of Raoyang Sag, Bohai Bay Basin, NE China

Xinshuai Li [a], Qingchun Meng [b], Jun Xie [a,*], Xiuwei Wang [b], Hong Chen [b], Minmin Shao [b], Yuzhi Zhao [b]

[a] College of Earth Science and Engineering, Shandong University of Science and Technology, Qingdao, 266590, China
[b] PetroChina Huabei Oilfield, Renqiu, 062500, China

ARTICLE INFO

Keywords:
Nearshore terminal fan
Seismic sedimentology
Sedimentary evolution
Raoyang sag
Shahejie formation

ABSTRACT

A nearshore terminal fan is a special water system formed in arid environments. The characterisation of its thin-channel sand bodies has long been a challenge restricting oil and gas exploration. This study takes the Suning area of the Raoyang Sag as an example and uses the principles of seismic sedimentology to conduct seismic sedimentary research on the nearshore terminal fan of the first member of the Palaeogene Shahejie Formation (Es1) based on three-dimensional seismic, logging, and core analysis. Seven fourth-order sequences (SQV7) were identified within Es1, deposited by a fluvial river system terminating at the contracting bank of a lake. Prograding terminal fan sedimentary facies on a gentle slope zone were observed in the root mean square seismic attributes after spectral decomposition. We have successfully resolved the sandstone within the studied terminal fan system using a 90° phase conversion of the seismic data and red-green-blue (RGB) fusion of the various seismic attributes. The upper subsegment of the Shahejie Formation developed extensive nearshore terminal fan sedimentation, and the seismic sedimentological response characteristics were mainly channel-like and strip-shaped geomorphic systems deposited on gentle slope zones, indicating distributary channels and distal basin sedimentation. This study enriches our understanding of nearshore fans and provides ideas for predicting favourable sand bodies in this type of sedimentary facies.

1. Introduction

A new play of thin sand reservoirs has emerged with the recent success of exploration and development in Raoyang Sag. Exploration results have proven that this area has a good source-reservoir-cap relationship [1,2], which is conducive for the large accumulation of oil and gas in the reservoirs developed within progradational geometries imaged in seismic data with various patterns, that is, oblique, S-type, S-type-oblique composite, and imbricate. During the deposition of the Palaeogene (P) Shahejie Formation (Es), the Raoyang Sag developed nearshore terminal fan deposits [3]. Nearshore terminal fan sands are often thin and can be difficult to directly resolve in the seismic profile because seismic reflection is usually influenced by the sedimentary interface of the adjacent strata and interference of the waveforms [4]. Lacking clear understanding of the nearshore terminal fan system can adversely affect reservoir

* Corresponding author.
E-mail address: xiejun0532@163.com (J. Xie).

https://doi.org/10.1016/j.heliyon.2024.e26584
Received 17 September 2023; Received in revised form 15 February 2024; Accepted 15 February 2024
Available online 27 February 2024

distribution prediction, restricting the exploration and development of this type of sedimentary body. Therefore, using seismic sedimentology [5,6] to study the sedimentary characteristics and planar distribution patterns of nearshore terminal fans systematically is of great significance for oil and gas exploration and development.

Recently, high-precision three-dimensional (3D) seismic technology has promoted the development of seismic sedimentology [7, 8]. Through the joint feedback of high-precision seismic data, modern sedimentary environments, and ancient outcrop sedimentary environment models, the 3D geometric shape [9], internal structure [10], and sedimentary processes [11] of sedimentary units can be determined. Geological bodies that are difficult to identify with vertical resolution can be identified through seismic horizontal resolution, and the description of the sedimentary plane distribution can be completed through well-seismic combination to predict the favourable distribution of lithological traps and fine characterisation of sand body morphology [12,13]. Seismic sedimentology has been applied to explore oil and gas in various sedimentary basins [14–17]. Prediction of sandstone diagenetic facies using conventional 3D seismic data in the Qingshankou formation in the Qijia area of the Songliao Basin was reported [18]. The distribution of reservoirs in the Xihu Depression of the East China Sea shelf basin was confirmed through seismic sedimentological research on the Oligocene Huagang Formation [19]. Study of the Spitsbergen Permian silicified carbonate rock carbonate sediments identified nine sedimentary microfacies through seismic sedimentology and determined their spatial distribution connections. Seismic sedimentology can more accurately characterize thin river sedimentary sand bodies [10].

A nearshore terminal fan is a type of sedimentation that occurs in a distributive fluvial system (DFS). The DFS is a new concept that refers to a sedimentary system in which the river enters the basin from a particular apex and is distributed radially. Its development is influenced by basin structure, climate, basin size, sediment source rock properties, and other factors. To study the DFS system, a fluvial fan was initially studied based on an impact fan [20]. In 2007, the definition and sedimentary model of fluvial fans were proposed by analysing the sedimentary facies model of the Dongpu Depression [21]. With the development of satellite imagery and remote-sensing observations, DFSs have attracted the attention of sedimentologists. Since 2015, many researchers have conducted in-depth studies on fluvial fans [22,23]. The appearance of nearshore terminal fans has changed the traditional continental sedimentary system that was dominated by alluvial fans, rivers, and lakes [24]. The Arman Formation of the Permian Rotliegen Group in the northeastern Netherlands includes a large sedimentary DFS and researchers have used seismic data to describe river channel characteristics in detail

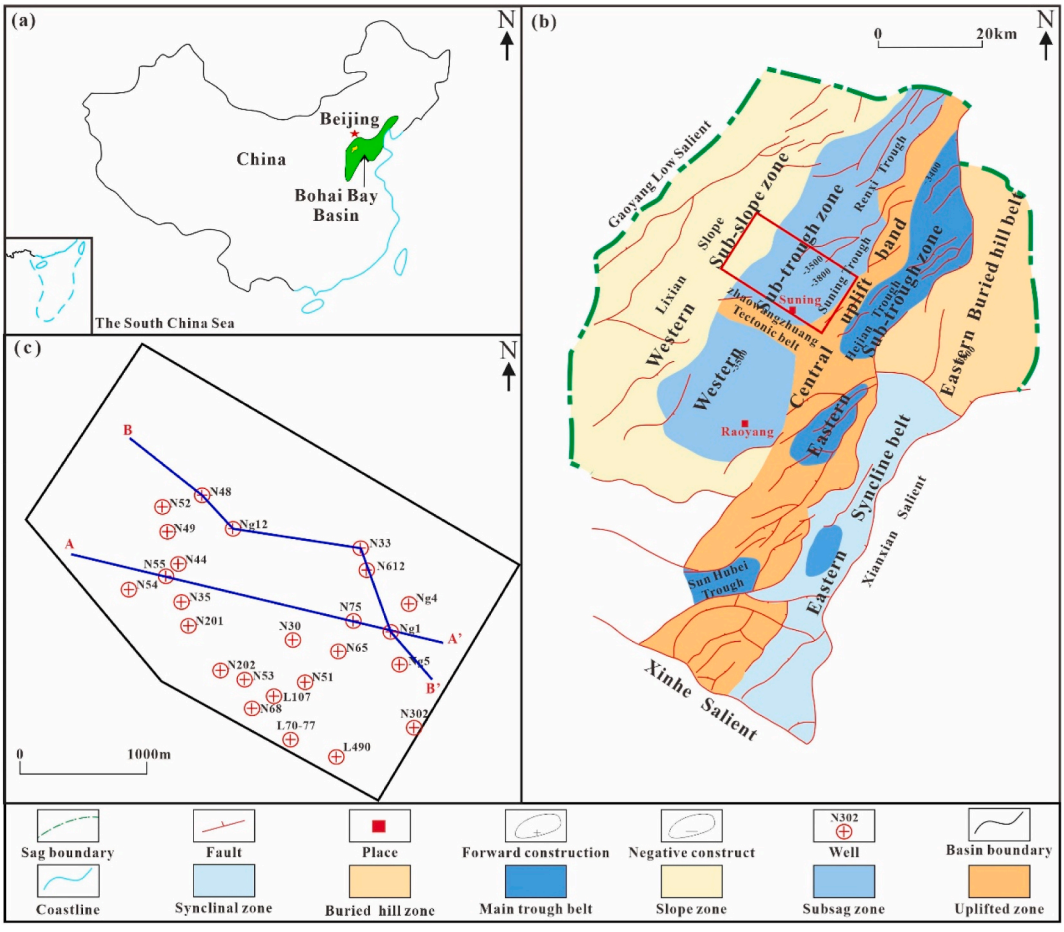

Fig. 1. Study area on Suning area of Raoyang Sag, Bohai Bay Basin. (a) Map of China; (b) Structural Map of Raoyang Sag, (c) Well location of the Suning area. This figure was drawn using Coreldraw, version 2018 (https://www.coreldraw.com/cn/).

[25].

The resolution of conventional seismic data is difficult to identify sedimentary sand bodies at the nearshore terminal fan because of nearshore terminal fan development in arid and semi-arid climates, flat terrain, weak downward cutting at the end of the river channel, shallow river channels with many horizontally connected areas, and thin foreset layers [26]. Because of the limited research on nearshore fans based on seismic sedimentary theory, many thin-layer sediments may be mistaken for other sedimentary systems. Seismic sedimentology can use lateral resolution (stratigraphic slicing) to compensate for the lack of vertical resolution, identifying thin sand bodies and providing an important theoretical basis for advancing the study of last-fan sedimentary systems [27].

The Shahejie Formation in the Suning area is a DFS of meandering channels over a large area with a low slope. The main sedimentary type was the nearshore terminal fan, and its sand body evolved rapidly in the horizontal and vertical directions. In addition, the well pattern densities in the study area vary significantly, and certain areas lack well control, resulting in an insufficient understanding of the geological conditions between wells. In this study, using core, logging, and 3D seismic data, and taking the Suning area as an example, the following research was performed: (1) The seismic sedimentology of the nearshore terminal fan was comprehensively analysed to clarify the seismic response characteristics. (2) This study examined the sedimentary evolution of the nearshore terminal fan during the contraction of the faulted basin, depicting the plane distribution of the distributary channel sand body, which provides a reference for seismic sedimentology research on the nearshore terminal fan in other basins.

2. Geological setting and stratigraphy

The Suning area in Raoyang Sag is rich in oil and gas resources. Unclear understanding of the lateral distribution of sand bodies in branch river channels affects oil and gas exploration and development. The systematic study of sedimentary facies in the Suning area is important for correctly understanding the sedimentary system in this area and has guiding significance for the distribution and prediction of sand bodies in favourable facies zones. The Suning area is situated in Raoyang Sag of the Jizhong Depression within the Bohai Bay Basin in China (Fig. 1a). This region is located in the central and southern parts of the Jizhong Depression, which is a half-graben characterised by a prominent boundary fault on its northeast side and a stratigraphic overlap towards the southwest slope. In the Suning area, located in the middle part of the Raoyang Sag, three normal structures converge: Dawangzhuang, Suning, and Hanjiacun (Fig. 1b) [28]. There are differences in well density in the study area, mainly located in the central and southern parts (Fig. 1c).

The main sedimentary stage of the Raoyang Sag is the Palaeogene, and the lithology of this stage is mainly continental clastic rock locally intercalated with carbonate rock. The Shahejie Formation experienced four stages: extension and deep depression, uplift,

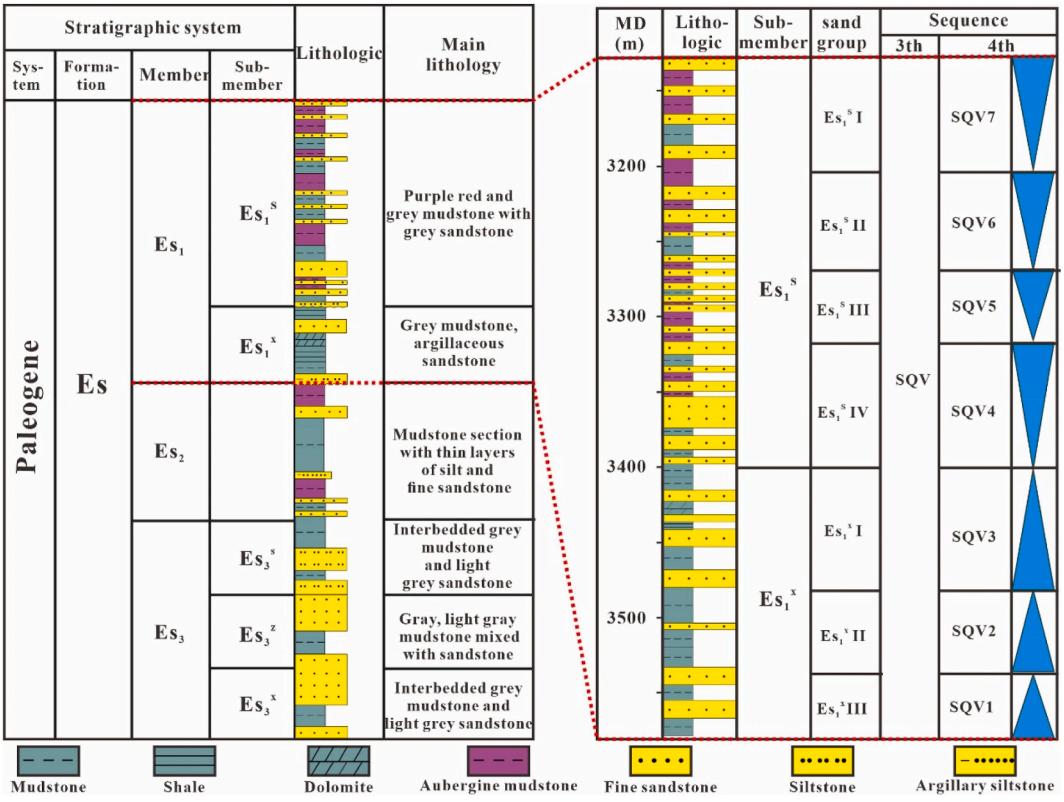

Fig. 2. Stratigraphic framework of the Paleogene Shahejie Formation.

extension and depression, and contraction and extinction [29]. The first member of the Shahejie Formation (Es_1) is the key horizon in this study. A set of thick river facies conglomerate sandstones is found above the top boundary of the Shahejie Formation, and below the interface is grey interbedded with purple red mudstone and fine sandstone, corresponding to the T3 interface. Es_1 slowly overlaps the second member of the Shahejie Formation (Es_2), which corresponds to the T4 reflection interface in the transition period from the fault depression period to that of the Himalayan first-episode basin, forming a large regional tectonic unconformity [30]. In the lower submember of the first member of Shahejie Formation (Es_1^x), the lake area was wide, but the water body was shallow and the deposition time was short. It then rose quickly, and the lake area shrank, entering the extinction period. The upper submember of the first member of Shahejie Formation (Es_1^s) was deposited to the depression extinction period, and abrupt changes occurred in the sedimentary facies belt and lithology. In areas with thickened strata, there are many short reflection progradational facies inclined toward the lake centre, creating a local unconformity. Finally, Es_1 was divided into a third-order horizon (SQV) and seven fourth-order sequences (SQV1–7, Fig. 2) corresponding to seven sand groups (Es_1^xIII–Es_1^sI). SQV1 corresponds to the lowstand domain, where a set of thick siltstones was deposited. SQV2–3 correspond to the lake transgression domain, and the lithology is mainly dark-grey mudstone, shale, calcareous sandstone, siltstone, and biological limestone. SQV4–7 of Es_1^s correspond to the highest stand. Red mudstone is observed in the lithology, reflecting an onshore oxidation environment.

3. Datasets and methods

The western gentle slope area of Raoyang Sag was covered by 200 km^2 of 3D seismic data. The data had line and trace spacings of 12.5 m and a sampling rate of 4 ms. The corresponding two-way time for the Shahejie Formation was approximately 2200–3500 ms. Analysing the seismic data volume using spectrum analysis, we observed that the dominant frequency of the Shahejie Formation was 20 Hz, with a frequency bandwidth of 10–60 Hz. The main horizons in the seismic profile show a stable event axis with clear faults. The signal-to-noise ratio of the seismic data was high, and the average longitudinal wave velocity of the formation was 3600 m/s. The estimated seismic resolution was 35 m, which was sufficient for interpreting the fine structure.

This study utilized ten coring wells to collect 823 representative core samples from the Palaeogene Shahejie Formation, covering a distance of 211.91 m. The seismic and logging data were obtained from the Huabei oil field.

Seismic sedimentology has improved the identification of sediment diffusion patterns and reconstruction of paleogeography through 3D seismic interpretation [31–34]. Key technologies [35] in seismic sedimentology include 90° phase transformation, spectral

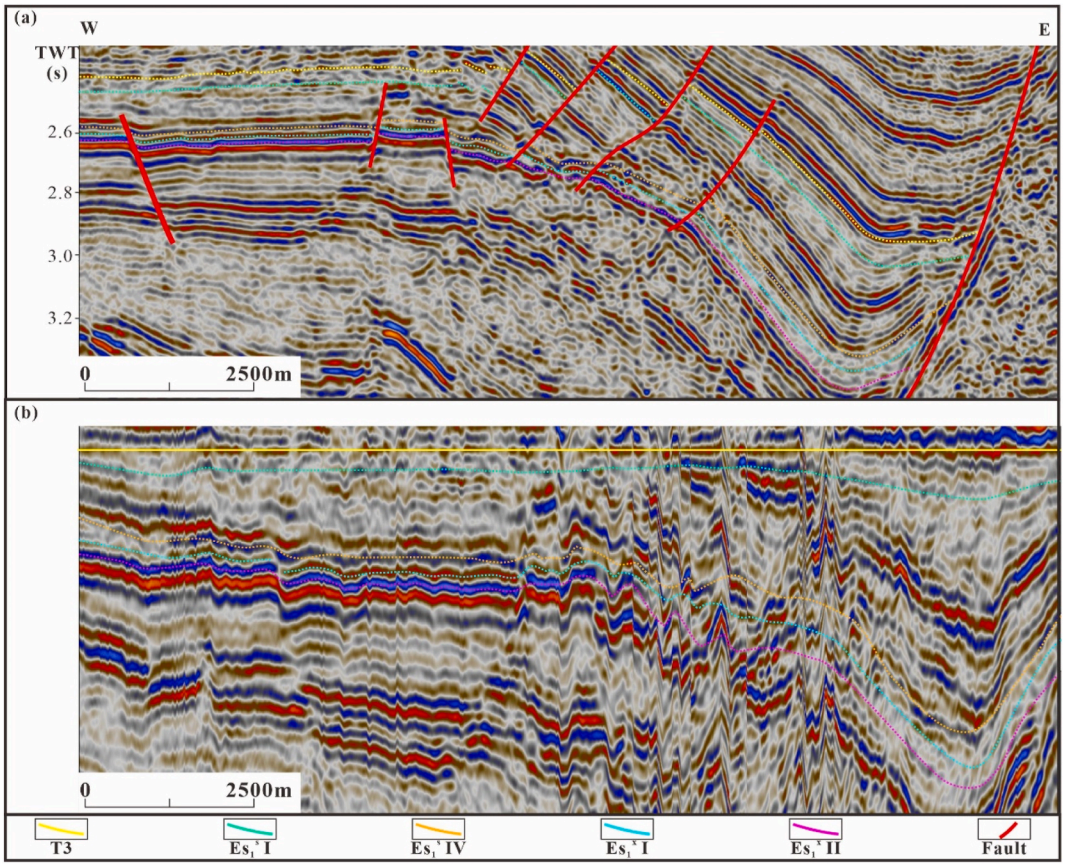

Fig. 3. Comparison of horizon levelling seismic profiles in the Suning area of Raoyang Sag.

decomposition, stratigraphic slicing, seismic attribute analysis, and seismic attribute fusion. The workflow of this study included four steps: (1) using layer flattening method to restore ancient landforms based on 3D seismic profiles and logging data, (2) analysing sedimentary and seismic facies using logging, lithology, and seismic data to establish an effective conversion of "seismic sedimentary facies," (3) conducting rock physics relationship analysis and comprehensive calibration of well seismic data based on 90° phase conversion and spectral decomposition to establish amplitude patterns and lithological relationships, and (4) using well control to analyse and predict favourable sand bodies by fusing seismic and red-green-blue (RGB) attributes of the sedimentary facies plane distribution.

4. Results

4.1. Sedimentological analysis

4.1.1. Provenance analysis

Provenance analysis is of fundamental importance in this research, as it guides the determination of sediment source locations, nature, migration paths, and distribution characteristics of sedimentary bodies [36,37]. The layer flattening method was used to investigate the palaeogeomorphology. Taking the sedimentary base level or maximum flooding surface as the reference base, the top and bottom surfaces of the studied sequence were selected, and the time difference was calculated. The proposed method is characterized by its simplicity and intuitiveness, making it conducive to swiftly and clearly presenting the landform prior to the deposition of the target layer [38,39]. Nevertheless, the layer flattening method solely accounts for the lateral variations of the strata, failing to fully

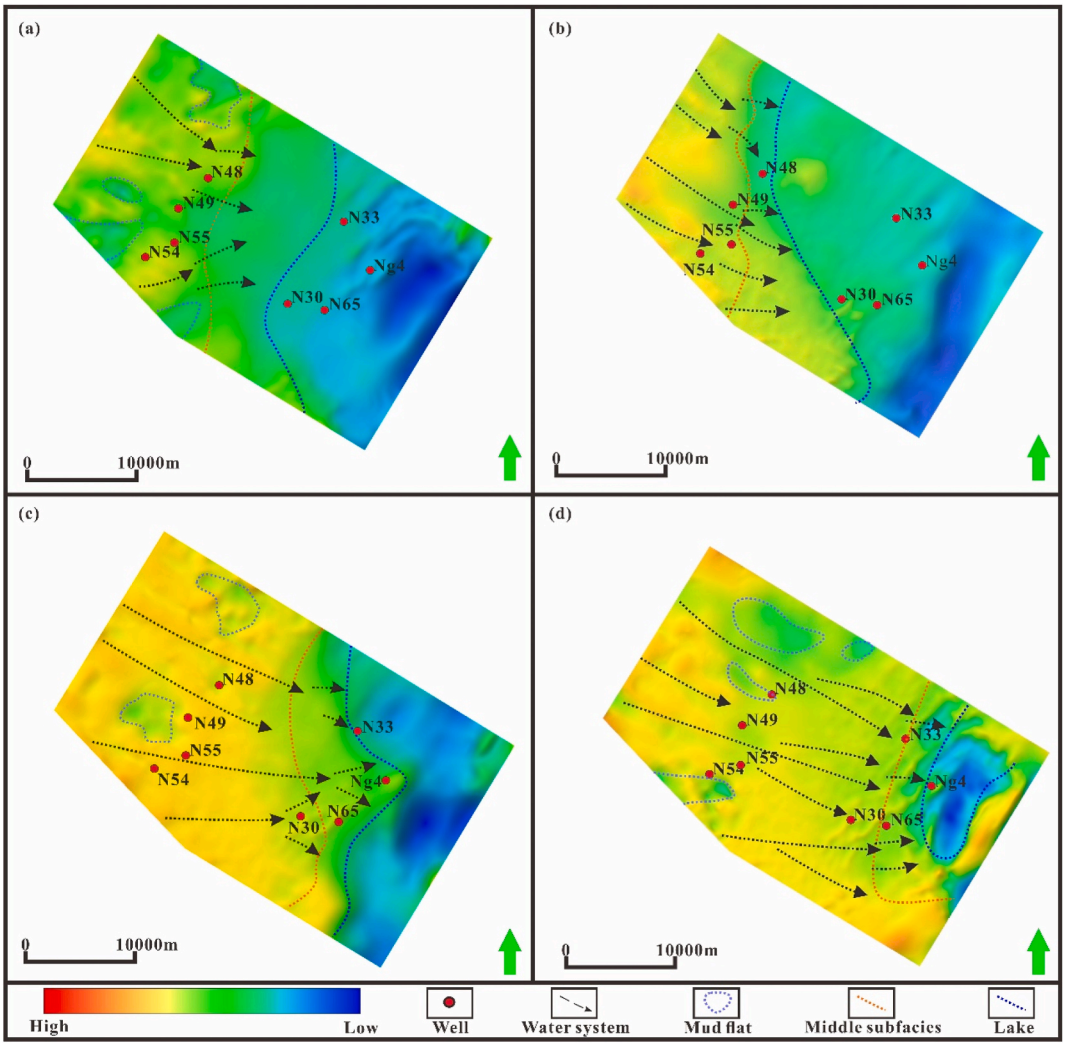

Fig. 4. Restoration of the ancient landform in the Suning area of Raoyang Sag. (a) Es_1^x II (SQV2) Restoration of ancient landforms, (b) Es_1^x I (SQV3) Restoration of ancient landforms, (c) Es_1^s IV (SQV4) Restoration of ancient landforms, (d) Es_1^s I (SQV7) Restoration of ancient landforms.

align with the geological evolution mechanism. In the presence of significant faults and folds, this approach may lead to computational inaccuracies in the determination of strata thickness and interface morphology.

Based on a comprehensive grasp of the geological context, which includes the structural evolution and basin architecture, a detailed elucidation of the seismic reflection layers of Es (SQV1–7) was performed to ensure the coherence of the seismic interpretation (Fig. 3a). Then, on the time domain seismic profile, flattening the T3 reflection interface and examining the ancient tectonic undulation pattern of Es_1 (SQV1–7), the flattened ancient topography presents a geomorphic pattern of high in the east and low in the west. The drilling data were comprehensively utilized to interpret ancient landforms on the flattened seismic profile. Subsequently, relevant software was employed to reconstruct the sedimentary paleogeomorphology (Fig. 3b).

Based on the developmental characteristics of ancient landforms in the Suning area, the geomorphic pattern of the study area has a suitable inheritance. There are two main sources of species in the research area: the western low rise of Gaoyang and southwestern low rise of Shenze. Owing to the continuous filling of sediment in the southwest, a gradual pattern of "high in the west and low in the east" is identified. During sedimentation period of the Es_1^x II (SQV2), the area experienced expansion and a depression occurred during. At that time, the lake was mainly located within the Suning Depression (Fig. 4a). During sedimentation of the Es_1^x I (SQV3), the lake basin experienced the largest lake intrusion. Although the lake surface expanded, the depth was shallow, and the duration was relatively short (Fig. 4b). Lacustrine sedimentation was the main type during the entire sedimentary period of Es_1^x (SQV1–3), with only a nearshore terminal fan developing in the eastern part of the study area. The basin was in an extinction period during the sedimentation of the Es_1^s IV (SQV4). The lake began to shrink, and owing to tectonic uplift, sedimentation of the nearshore terminal fan developed widely (Fig. 4c). During the sedimentation of the Es_1^s I (SQV7), tectonic uplift continued to strengthen, the lake basin nearly disappeared, and a distributary channel system developed throughout the area (Fig. 4d).

4.1.2. Lithological characteristics

Through the analysis of rock debris logging and core observations, the predominant colours of the mudstone in the study area were found to be brownish- and purplish-red. These mudstone deposits are extensively found in Es_1, indicating oxidised sedimentary environments. Based on this information, the core samples were classified and statistically analysed (Fig. 5). The sandstone types in Es_1^x of the research area primarily consist of feldspathic and lithic feldspathic sandstones. These sandstone types had quartz volume fractions ranging from 45% to 63%, with an average volume fraction of 53.6%. The volume fraction of feldspar varied from 23% to 51% with an average volume fraction of 36.9%. Rock fragments were relatively scarce, with an average volume fraction of 9.6% (Fig. 5a). In the Es_1^s of the study area, feldspathic and lithic feldspathic sandstones were predominantly observed. This sandstone type had a quartz volume fraction ranging from 34% to 59%, with an average volume fraction of 47.1%. The volume fraction of feldspar varied from 23% to 52% with an average volume fraction of 42.1%. Additionally, the volume fraction of the rock debris ranged from 2.3% to 23%, with an average volume fraction of 10.8% (Fig. 5b). The degree of rock weathering in the study area is moderate, with good sorting ability and subroundness. The grain-size distribution of the Es_1^s sandstone in this region was primarily influenced by jump formation, indicating

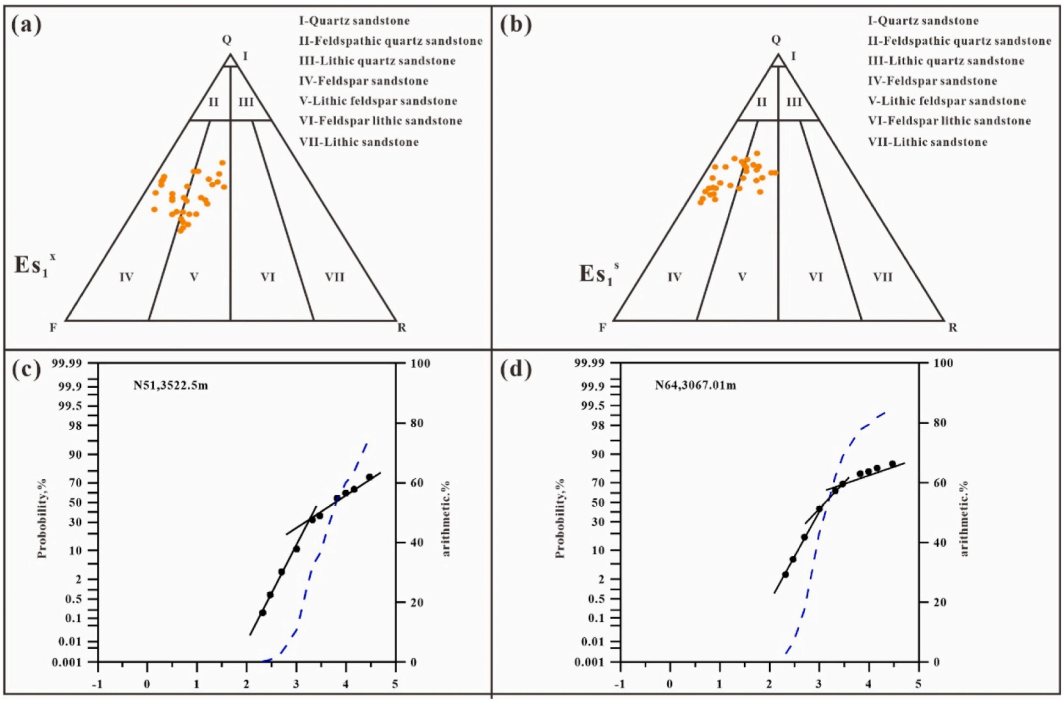

Fig. 5. Lithology triangle figure and grain size distribution curves of Es_1 in the study area. (a) The triangular plot of Es_1^x sandstone types, (b) The triangular plot of Es_1^s sandstone types, (c) N51, 3522.5 m, two-stage, (d) N64, 3067.01 m, two-stage plus transitions.

significant hydrodynamic characteristics. Suspended components constitute a volume fraction of 10–20%, and the slope is greater than 60%, whereas rolling components are scarce. The dominant types of grain-size probability accumulation curves are two-stage and two-stage plus transitions, reflecting the hydrodynamic characteristics of the traction flow (Fig. 5c and d).

Based on the analysis of the core and logging data, nearshore end-fan sediments were identified in the study area, with microfacies including distributary channels, channel overflow, point bars, mudflats, and distal basin microfacies in the subfacies, as well as sandbar and beach facies of the coastal and shallow sediments. Es_1^x is primarily composed of thick grey and light grey siltstones interbedded with grey sandstone and mudstone. Low cross-bedding sand bar sedimentation (Fig. 6a) and sand–mud interbedded beach sedimentation (Fig. 6b) were observed in the rock core. Es1s primarily included sedimentation in the nearshore end fan, and the distributary channel was the main sand body development area in the nearshore end fan. The lithology is mainly fine sandstone and siltstone, with clear erosion surfaces (Fig. 6c) and visible water-flow sand bedding (Fig. 6d). Spot bar sedimentation can be seen locally in the river channel, with fine sandstone and medium sandstone as the lithology and developed oblique bedding (Fig. 6e). Water overflow can be divided into near- and far-channel overflow based on distance from the river. The near-channel overflow developed mud and gravel at the bottom (Fig. 6f), whereas the far-channel overflow was primarily composed of mudstone interbedded with thin layers of fine sandstone and siltstone (Fig. 6g). Mudflat facies mainly developed in low-lying areas between distributary channels, with mudstone as the main lithology and thin sandstone interbedded with block-like bedding (Fig. 6h). The microfacies of the remote basin were weakly affected by river action, with the development of wavy and vein-bedding (Fig. 6i).

4.1.3. Logging facies characteristics

Through analysis of core wells in the study area, the gamma ray (GR) and spontaneous potential (SP) morphology and characteristics, corresponding to typical sedimentary microfacies, were identified. Five main logging facies were observed within the study interval [40]: funnel-, box-, bell-, finger-, and baseline-shaped, compared with SP, GR has obvious serration characteristics (Fig. 7). Funnel-shaped SP logging facies are commonly found at the edges of lake basins where sediments are heavily influenced by lake waves and coastal currents. These facies exhibit abrupt changes at the top, gradual changes at the bottom, and anti-rhythms vertically. The

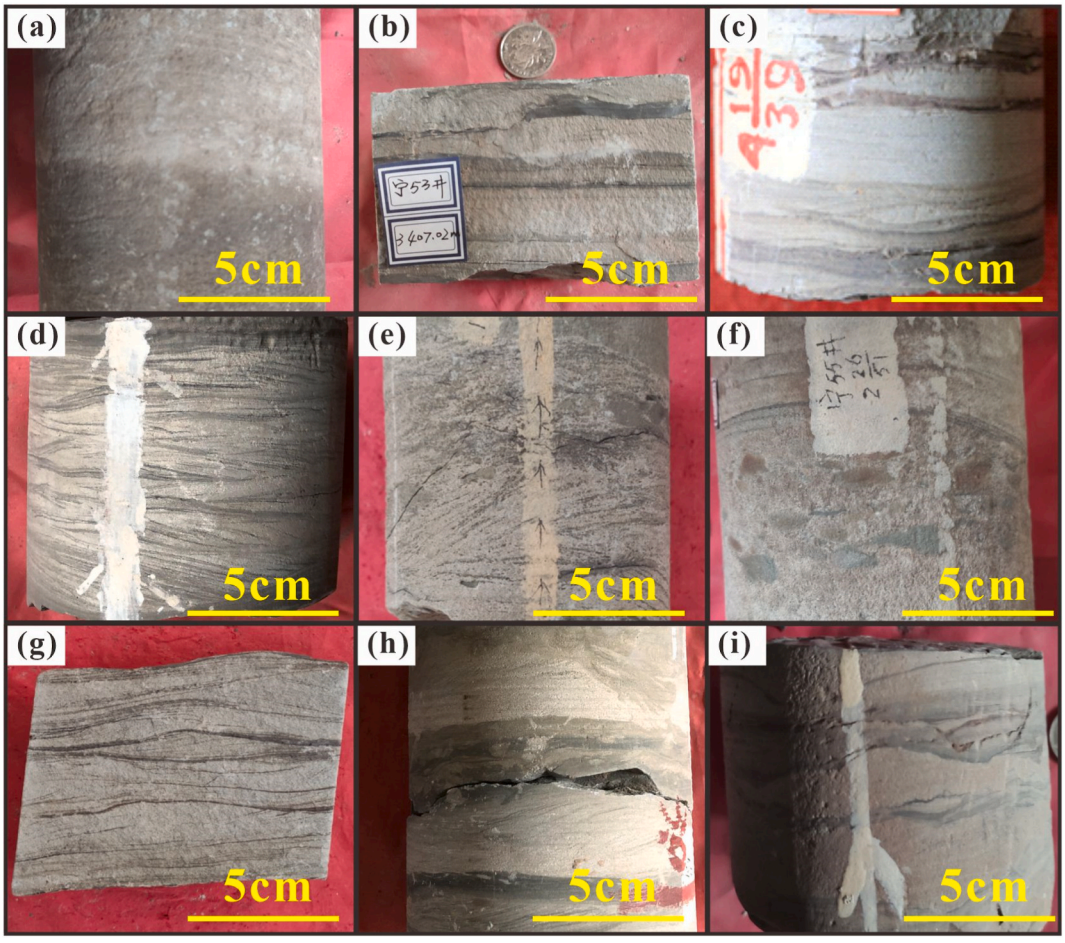

Fig. 6. Images of a typical core. (a) N55, 3352.8 m, (b) N53, 3407.02 m, (c) N32, 3596.4 m, (d). N48, 3500.9 m, (e) N50, 3112.9 m, (f) N55, 3262.3 m, (g) N49, 3292.28 m, (h) N62, 3322.53 m, (i) N66, 3500.9 m

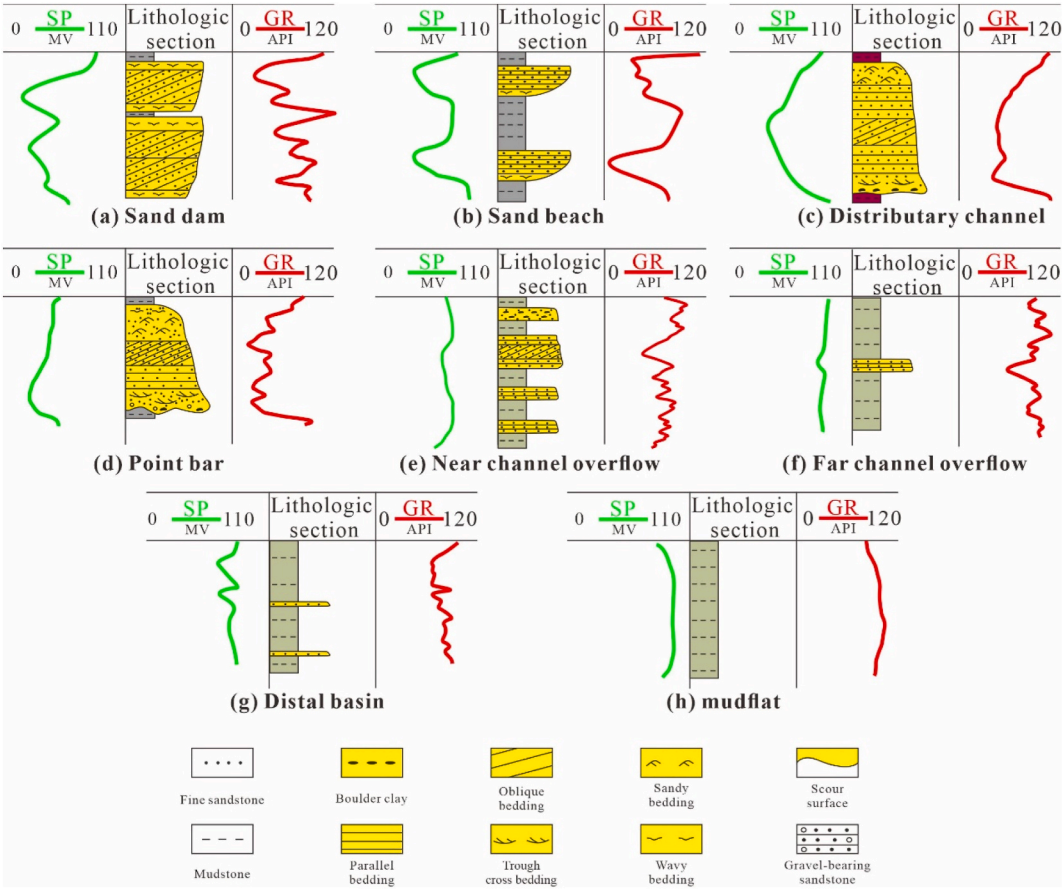

Fig. 7. Images of a typical logging facies.

GR logging facies also displayed clear toothing, indicating sandbar facies with sand-mud interbedding (Fig. 7a). In cases where the thickness of a single sand body is small and sand-mud interbedding is more frequent, the SP and GR logging facies are typically medium- or low-amplitude finger shaped or serrated, reflecting beach facies (Fig. 7b). The SP and GR logging facies of distributary channels are mainly box shaped. Box-shaped logging facies are characterised by abrupt changes at the top and bottom and are vertically superimposed by 2–3 positive rhythms, resulting in slightly dented logging facies that indicate distributary channel sedimentation (Fig. 7c). The SP logging facies are mainly bell-shaped, and the GR facies is toothed bell-shaped, reflecting point-bar deposits associated with lateral accretion (Fig. 7d). River overflow, which occurs when sandy sediment spills over the riverbank owing to erosion during flood periods, influences the logging facies, which vary based on the distance from the river. The SP logging facies is smooth and low amplitude funnel shaped, while the GR logging facies is finger shaped and small toothed bell shaped, indicating the vertical superposition of multiple positive grain sequences and suggest near-channel overflow (Fig. 7e). In contrast, SP logging facies is low-amplitude tooth shape or flat shape and GR logging facies have obvious toothed shape, indicating the far-channel overflow of a thin single sand body (Fig. 7f). These facies represent distal basin microfacies located at the front edge of the river overflow and far from the source. The lithology in this area primarily consists of reddish-brown and greyish-green mudstones with a low sandstone content, resulting in the formation of weak toothed baseline logging facies in SP and GR logging facies (Fig. 7g). The baseline logging facies point to the direct floodplain of the nearshore terminal fan and are primarily composed of mudstone with a low sand content (Fig. 7h).

4.1.4. Single well facies characteristics

Sedimentary structure is a direct reflection of the sedimentary environment and hydrodynamic conditions in rocks and an important indicator for distinguishing sedimentary environments and dividing sedimentary facies, subfacies, and microfacies [41]. The core layer of Well N53 is located in the Es_1^x II–Es_1^x I (SQV2–3), with the GR and SP curves mainly being box- and loophole-shaped. The sedimentary structure was mainly composed of oblique bedding to form anti-rhythmic sedimentation, mainly developing beach and sandbar facies in the shoreline shallow lake facies. The Es_1^x II (SQV2) developed light grey fine sandstone interbedded with small sections of mudstone, developing two sets of oblique bedding sandbar sand bodies. two sets of sand bars with oblique bedding planes disturbed by waves developed at the bottom and top of the Es_1^x I (SQV3), and parallel bedding beach facies developed in the middle (Fig. 8).

L70–77 were located in the western gentle slope area of the research area, with the core layer located in the Es_1^5 III–Es_1^5 I (SQV5–7). The GR and SP curves were mainly bell-shaped, with multiple positive rhythmic sediments, in the middle of the nearshore terminal fan. The microfacies were dominated by distributary channels, near-channel overflow, and far-channel overflow. The Es_1^5 III (SQV5) is composed of variegated mudstone and grey fine sandstone, with parallel bedding and water flow sand ripple bedding developed in sequence, forming a large set of channel overflow sand bodies, whereas the overall appearance of the Es_1^5 II (SQV6) is a frequent sand mud interbedded sandy mudstone, which is a near-channel overflow. Distributary channel sand bodies, which have mud-gravel erosion surfaces, are present in the middle and bottom. There are grey-green and brown mudstones in the upper part of the channel, which are mudflats. The top of the Es_1^5 I (SQV7) is an interbedded layer of sandy mudstone and downwards is a distributary channel sand body. The bedding structure includes water-flow sand bedding, parallel bedding, and a scouring surface containing mud and gravel (Fig. 9).

The vertical distribution of the sedimentary facies in E_{S1} (SQV1–7) was revealed by the cross-well profile along the provenance direction (Fig. 10). The shore-shallow lake subfacies primarily developed in Es_1^x III–I (SQV1–3). The lake is shallow, wide, and primarily composed of interbedded fine grey sandstone and mudstone. The distributary channel developed primarily east of the study area, continuing to extend in Es_1^5 (SQV4–7), spot bars and channel overflow microfacies developed near the meandering channel. However, the channel never entered the lake, forming fine sandstone distal basin microfacies near the lake bank.

4.2. Seismic-sedimentology analysis

4.2.1. Seismic facies analysis

Seismic facies analysis is the sum of the rock sedimentary facies on the seismic profile and is the seismic characteristic formed by the sedimentary environment [42–44]. The sedimentary microfacies of the nearshore terminal fan include the far basin, distributary channel, mudflats, channel overflow, and point bars. The distributary channel is large in scale and mostly composed of superimposed channel belts with a channel bandwidth of approximately 1000 m. It reaches the centre of the basin, where the terrain becomes gentle, and terminal fan deposits are formed. The seismic facies in most areas are characterised by weak amplitude, sub-horizontal, and discontinuous reflection, and the characteristics of progradational facies can be identified in locally thicker areas (Fig. 11). Local distributary channels can also recognise point bar sand bodies, which are lens-shaped in the seismic facies (Fig. 11). The seismic facies of the mudflats are characterised by parallel and subparallel reflections. Because of the weakening river channel energy, it cannot be cut deeply. During the flood period, the river channel overflows to form a channel overflow. Seismic facies are characterised by subparallel chaotic reflection changes. Based on the distance from the river channel, they can be divided into near-channel and far-channel overflows. The mud content of the far-channel overflow was high (Fig. 11). With the extension of the distributary channel, the channel density decreased, and sedimentation transitioned to the distal subfacies, forming the distal basin microfacies, which belong to the transition zone from lacustrine facies to lacustrine facies. The seismic facies showed large areas of low- and medium-amplitude subparallel reflections (Fig. 11).

4.2.2. Phase adjustment of seismic data

According to the well data, the depth of the reservoir is greater than 3000 m, and the thickness of the sand body is less than 15 m. Seismic data with 90° phase can improve the interpretation of lithological and stratigraphic results. After 90° phase conversion, rock physical relationship analysis and spectrum decomposition must be conducted to establish the relationship between seismic facies and

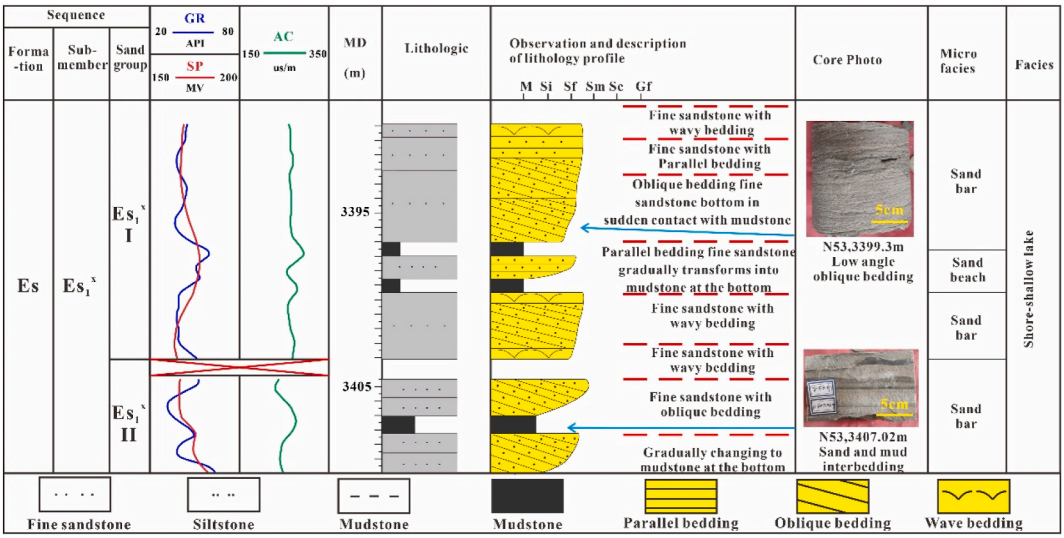

Fig. 8. Single well facies of Well N53.

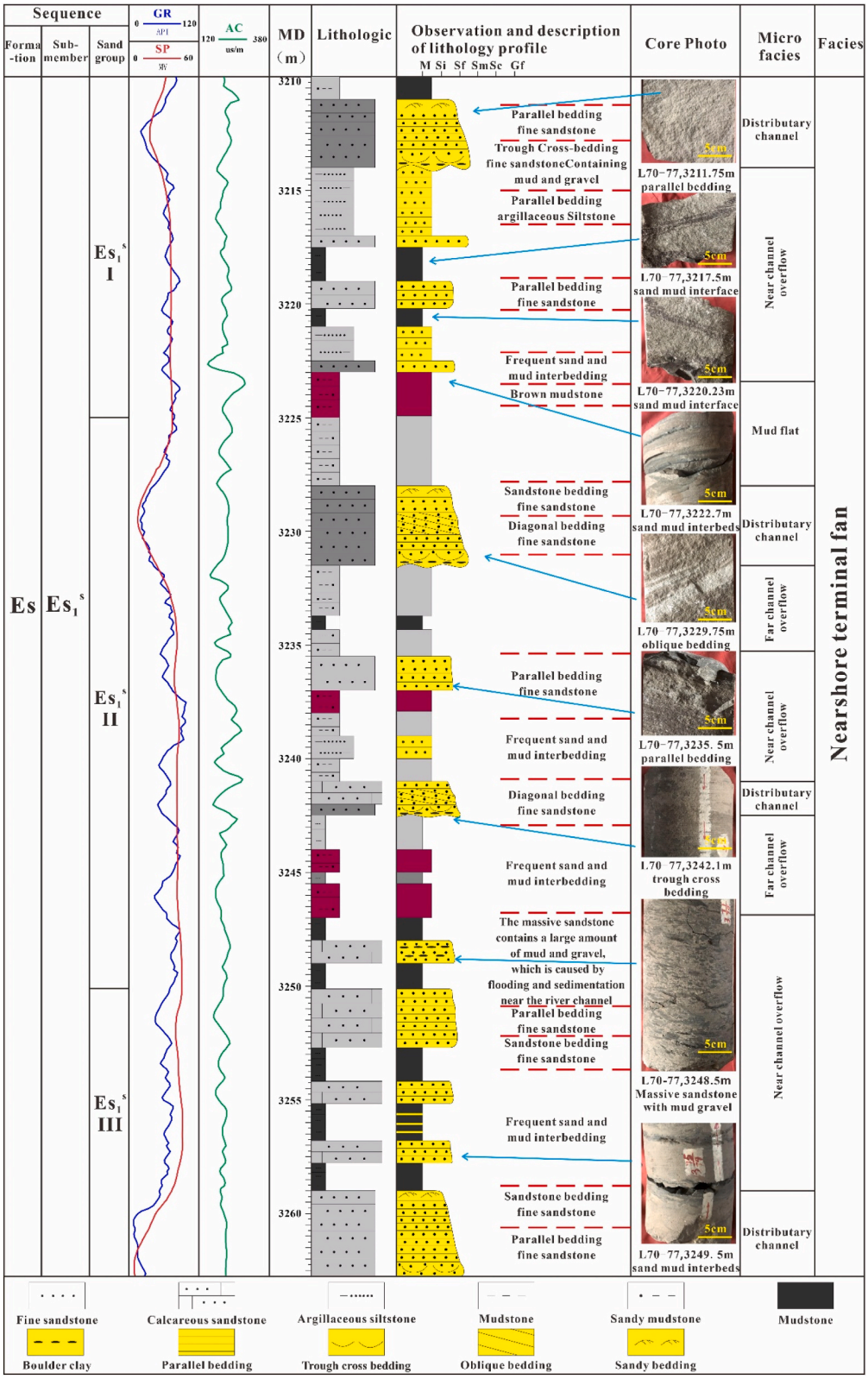

Fig. 9. Single well facies of Wells L70–77.

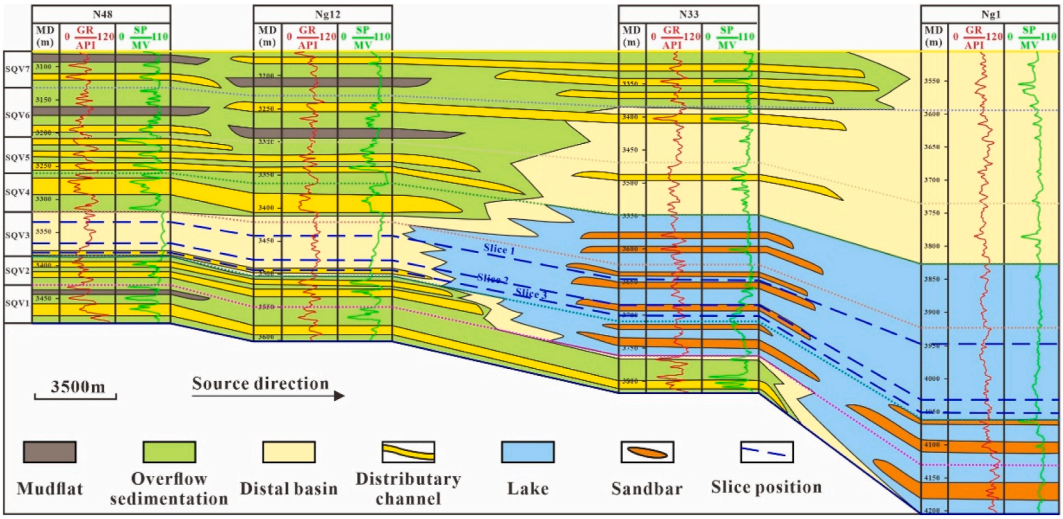

Fig. 10. Correlation of sedimentary facies of Es (SQV1–7) across the study area using wireline logs.

Sedimentary type		Seismic facies characteristics	Seismic facies profile
Middle subfacies	Distributary channel	Filling shape, Medium amplitude, Medium frequency.	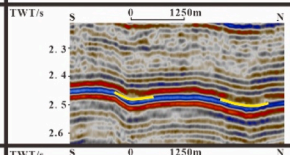
	Overflow of waterways	Mat shaped, Medium low amplitude, Medium low frequency Chaotic - parallel sub parallel reflection.	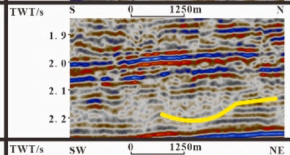
	Point bar	Medium to strong amplitude, Lenticular reflection.	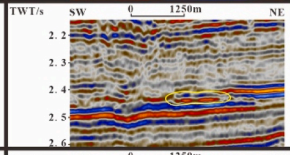
	Mudflat	Sheet shaped, Medium to low amplitude, Medium frequency, Parallel sub parallel or chaotic reflection.	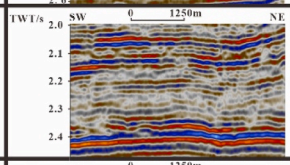
Distal subfacies	Distal basin	Mound shaped, Medium low amplitude, Medium low frequency, Subparallel or chaotic reflection	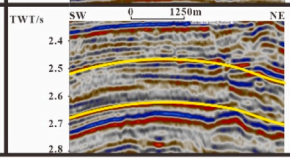

Fig. 11. Sedimentary and seismic facies of the Shahejie Formation in the study area.

lithology [45]. In this study, the relationships among lithology, wave impedance, and amplitude were established by generating a natural gamma - wave impedance crossplot, and the seismic reflection polarity or amplitude of a specific lithology was predicted. The lithology of the study area consists of mudstone, sandy mudstone, argillaceous sandstone, and sandstone. The data points for the different lithologies are located within a specific wave impedance range. Specifically, sandstone mainly exhibits a high wave impedance, whereas mudstone mainly exhibits a low wave impedance. The transitional lithology shows a concentrated multiple wave impedance range from 9200 to 10,400 kPa*s/m (Fig. 12a). The 90° phase conversion leads to an enhanced alignment between the event axis and the logging curve. The sand body exhibits a near correspondence to the seismic trough (negative amplitude), while the high natural gamma values align with the seismic peak (positive amplitude) (Fig. 12b). By observing the relationship between the rock

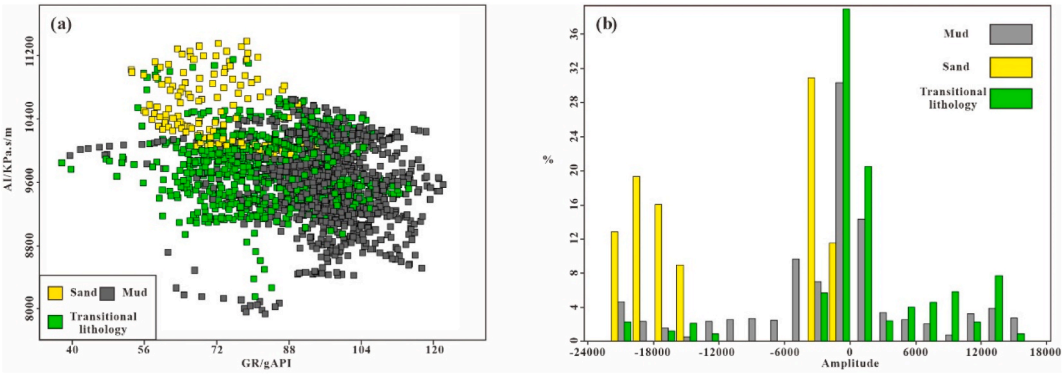

Fig. 12. Mudstone Wave Impedance and Natural Gamma. (a) Intersection diagram of GR and AI, (b) Lithological amplitude distribution map.

layers and seismic reflection event axis, the determination can be made as to whether the event axis corresponds to a single lithologic layer or a lithologic composite layer. The study area had a small range of facies zones and frequent phase transitions. There was no correspondence between a single rock layer and the reflection axis. The event axis represents only the change in the average wave impedance, that is, the negative-amplitude partial sand facies and positive-amplitude partial mud facies (Fig. 13a). When comparing the matching relationship between the amplitude and GR response at different frequencies, the matching degree between the GR and amplitude was the best when the frequency was 45 Hz (Fig. 13b and c). Through spectral decomposition technology, the amplitude

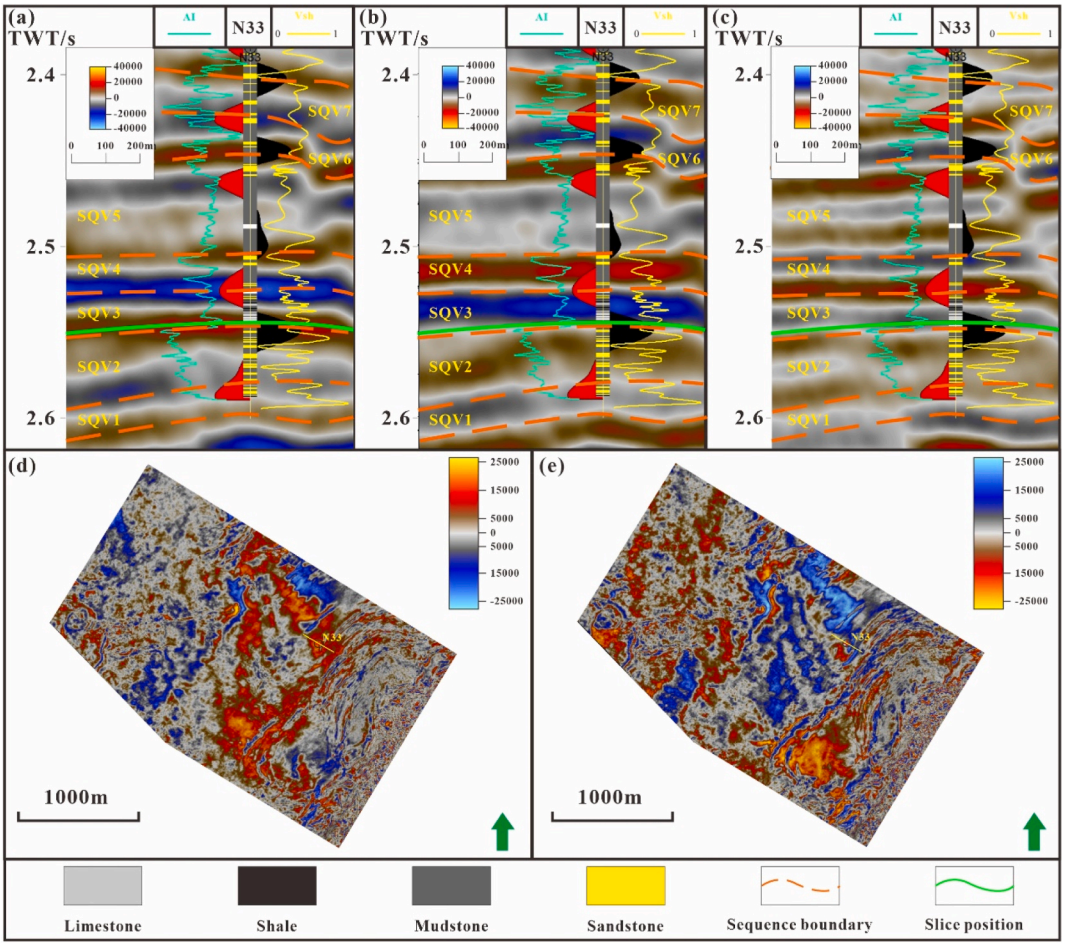

Fig. 13. Comparison of seismic events before and after the 90° phase conversion in Es_1 in the Suning area. (a) 0° phase seismic profile, (b) 90° phase seismic profile, (c) 90° phase profile of 45Hz seismic body, (d) 0° phase stratigraphic slice, (e) 90° phase stratigraphic slice.

response characteristics of thin sand body targets were enhanced, and the comprehensive superposition interference effect of thin sand body interbedding was reduced. Taking well N33 as an example, there is no clear correspondence between the sandstone and mudstone phases and the seismic profile on the same phase axis. For example, the sandstone section of the Es_1^x I (SQV3) is not aligned with the mudstone section of the Es_1^s III (SQV5) (Fig. 13a). In the 90° phase seismic profile of the 45 Hz frequency body, the mudstone exhibits a blue peak, indicating low AI and high Vsh, whereas the sandstone displays a red trough, representing high AI and low Vsh. In the 90° phase seismic profile of the 45 Hz frequency body, mudstone has a blue peak, whereas sandstone shows a red trough (Fig. 13c). The 90° phase seismic profile optimises the specific relationship between seismic amplitude and lithology, makes the profile closer to the wave impedance profile, and improves the interpretability of seismic data. The 90° phase slice can better identify the changes in sand body sedimentary boundary. In the Es_1^x I (SQV3) lacustrine intrusion system tract, the channel deposition is advancing eastward, with the red amplitude corresponding to the distributary channel, the morphological representation of GR and SP curves is box-shaped or bell-shaped. The lake sediments in the East can be interpreted as shallow lacustrine muddy facies. There are banded negative amplitudes in the blue positive amplitudes, indicating beach bar. The sedimentary boundary is more obvious than the formation of phase 0° (Fig. 13d and e).

4.2.3. *Interpretation of seismic attributes*

Seismic and logging data are the two primary data types of significance. Despite its low resolution, seismic data exhibits wide range and good lateral continuity [46]. It interprets seismic attribute slices under logging constraints. Suitable interpolation between the two isochronal interfaces was used to achieve stratigraphic slicing. It provides high-resolution slices and accurate detection of sedimentary

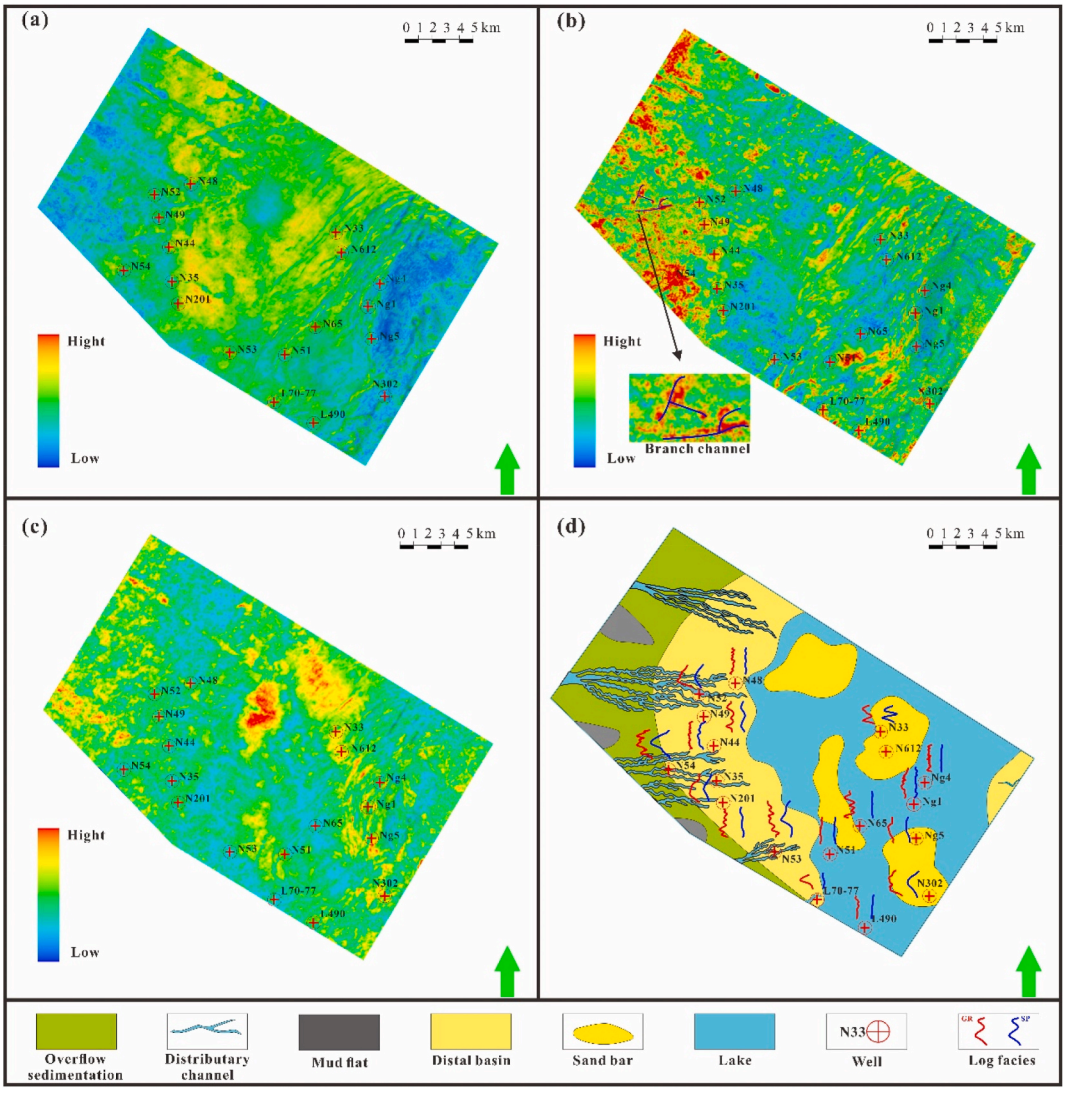

Fig. 14. Sedimentological interpretation of Es_1^x I (SQV3) in the Suning area. (a) Es_1^x (SQV3) interlayer RMS, (b) 45Hz RMS Stratal Slice (Slice position as shown in Fig. 10 Slice 1), (c) 30Hz RMS Stratal Slice (Slice position as shown in Fig. 10 Slice 2), (d) Sedimentary facies distribution.

interfaces, as well as a large number of slices controlled by a sequenced framework, which is useful for analysing sedimentary evolution [47]. The sedimentary interpretation of the study area was performed by optimising the plane attributes that were consistent with the thickness of the well-point sand body.

Based on the extraction of the inter layer RMS amplitude attribute of the Es_1^x I (SQV3), the distributary channel sand body is thin, and the distributary phenomenon is frequent. It is difficult to make a horizontal comparison; the response characteristics are weak, and the entire layer is blue-green, whereas the deposition of the distal basin microfacies occurred at the front edge of the nearshore terminal fan and deposited with the weakening of hydrodynamic force. The overall amplitude is weak, the single sand body corresponds to a thin layer of argillaceous siltstone, and the natural gamma and natural potential are mostly flat, but the horizontal distribution is relatively continuous, and it is easy to identify yellow or green reflections distributed along the lake shore on the interlayer root mean square (RMS) attribute (Fig. 14a). The response characteristics of shallow shore lacustrine deposits in stratigraphic slices are mainly shown in low-value blue in the thin sections, which are concentrated in the eastern depression, with shallow lake water and large water areas. To identify the distribution of river sand bodies better, we selected a smaller time window to extract the RMS vibration attributes of the Es_1^x I (SQV3) based on spectral decomposition. Compared with the 30 Hz slice, the 45 Hz slice can better identify excessive changes in sedimentary facies, and the 45 and 30 Hz slices can identify the 20 and 30 m sand bodies, respectively. The Es_1^x I (SQV3) sedimentary facies are dominated by shoal and bar facies, and the nearshore terminal fan is developed only in the east (Fig. 14d). Based on the GR calibration, it can be determined that during this period, the development of bars and embankments is relatively prominent, with a single sand body thickness of 4–5 m. The logging facies are characterized by serrated box shapes. The river channel usually starts from the southwest and develops to the northeast. After spectral decomposition of the data volume, a composite river channel amplitude anomaly was observed on the 30 and 45 Hz stratigraphic slices, GR displays a tooth-shaped funnel form. The overall response characteristics weakened from east to west, consistent with the distribution characteristics of the river channel. Among them, 30 Hz corresponds to the best characterisation of shallow shore sand dams, 45 Hz shows better characteristics of the river channel, and the amplitude intensity reflects the superposition of river water and sediment in different periods (Fig. 14b and c).

The Es_1^s III–II (SQV5–6) developed extensive distributary channels, the nearshore terminal fan shared the Es_1^x (SQV1–3) progradation direction, and the lacustrine facies was only present in the eastern groove area (Fig. 15a and b). Owing to the reduction in sedimentary thickness, the reflection of the seismic profile is now dominated by subparallel reflection, with a large number of worm-like amplitude reflections in the stratum slice, the well logging is often described as toothed funnel-shaped, smooth ovoid, or broad finger-shaped. In contrast to Es_1^x (SQV1–3), there are strongly reflective channel bodies in the constant-amplitude slices, which are considered channel complexes superimposed by multiple sedimentary periods (Fig. 15b). Near the lakeshore, there is a high-amplitude superimposed response characteristic, which suggests that during intermittent floods, most areas were submerged and the water flow was no longer restricted by the river channel, resulting in the formation of distal basin microfacies overflow sedimentation (Fig. 15a). The floodplain facies are widely developed in the central subfacies, represented by weak amplitude reflection characteristics in the central region; the inversion of the amplitude slices is shown in blue. The central subfacies is widely developed. Apart from the main distributary channels, it mainly consists of overbank deposits characterized by medium to weak amplitude reflections. In the areas away from the channels, the seismic slices appear blue, and the well logging indicates weakly toothed or straight baselines.

Traditional seismic interpretation uses stratum slicing technology to extract amplitude attributes along the target layer, reflecting the change rate of longitudinal wave impedance and making it easy to identify the geological body; however, when the target layer is thin, a single attribute is difficult to explain [48]. RGB volume fusion technology combines multiple attribute volumes to depict the distribution characteristics of sand bodies of different sizes and has a prominent effect on describing different lithological boundaries and river morphologies [49]. Taking the Es_1^x I (SQV3) as an example, during this period, the central and distal sub-phases of the nearshore terminal fan was dominant, and the western river channel was distributed in radial strips. As the river flowed eastward, the hydrodynamic conditions weakened and were no longer restricted by the river, thus forming distal subfacies. The integration of the RMS, 30 Hz, and 45 Hz seismic bodies clearly revealed the overflow sand bodies of the distributary channels and waterways, as well as the distal basin microfacies. In the attribute fusion slice, there was a green strip response in the eastern part of the study area, separated by a dark response, and its distribution was consistent with that of distributary channels and mudflats. There were horizontally distributed bands in the middle, with a green response as the distal subfacies and an enhanced dark response in the eastern groove area entering the shallow lake facies (Fig. 16a and b).

5. Discussion

When utilizing seismic and logging data to predict and characterize favourable sand bodies, variations in the comparison results can occur because of the disparity between the low frequency of seismic signals and the high resolution of geophysical logging data. Therefore, this study standardizes the scale of logging data by selecting log data from matched wells. Based on 90° phase conversion and spectrum decomposition techniques, the study establishes the corresponding relationship between seismic amplitudes and logging lithologies through petrophysical analysis to improve the prediction accuracy of sand bodies between wells. Prediction of sand distribution using seismic attributes is a widely used method [50]. In this study, a 90° phase conversion of the seismic profiles was performed before extracting seismic attributes, and the corresponding relationship between the transformed seismic profiles and lithology was analysed. Sandstone primarily corresponded to the trough of the seismic section after the 90° phase conversion. Based on this feature, corresponding attributes for the 90° phase conversion seismic profiles were extracted, and the amplitude fluctuation of attribute slices marked the distribution and overlap patterns of sandstone layers. The sandstone and mudstone had high- and low-wave impedances, respectively. Next, we examined the rock formation to determine the state of lithological overlap corresponding to the seismic reflection in-phase axis. When recognising specific targets, frequency division and fusion can highlight their spatial

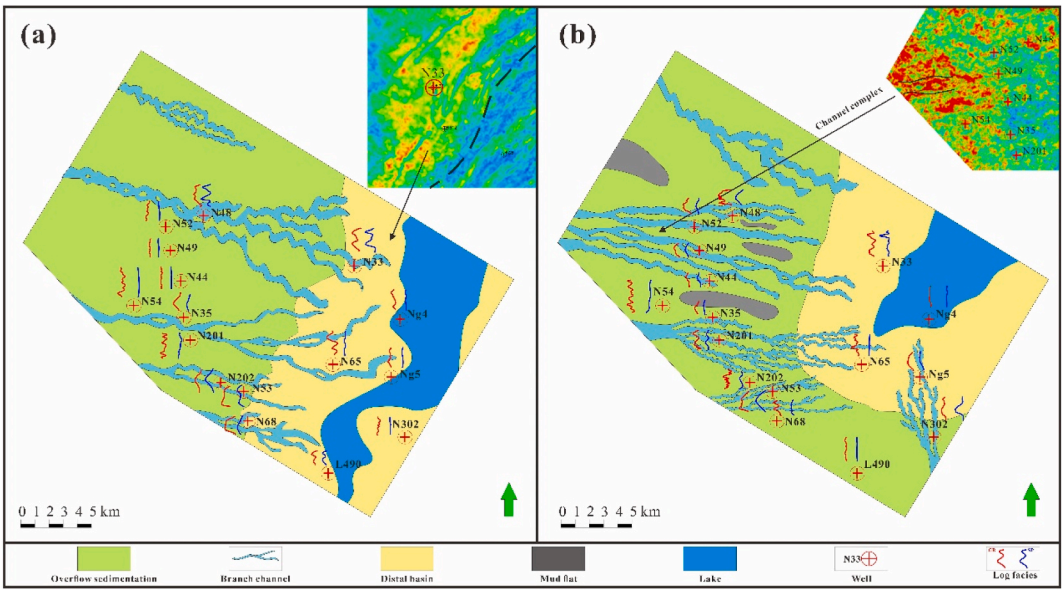

Fig. 15. Sedimentological interpretation of Es_1^s Seismic in the Suning area. (a) Es_1^s III (SQV5) Sedimentary facies distribution, (b) Es_1^s II (SQV6) Sedimentary facies distribution.

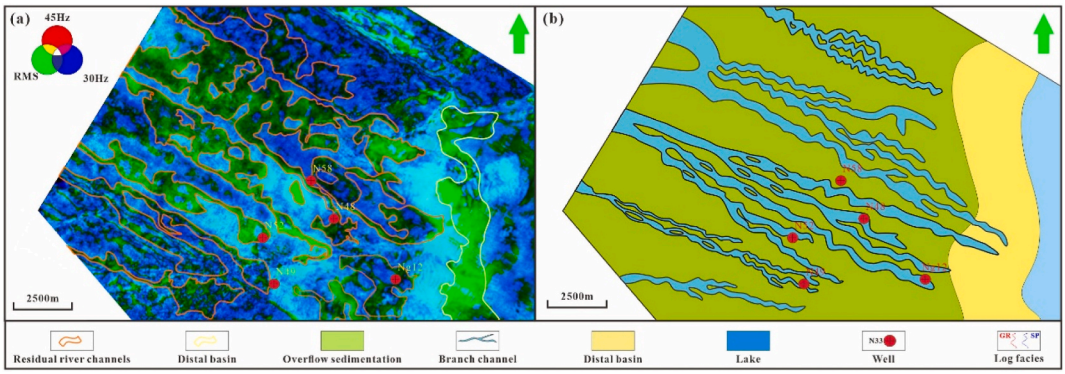

Fig. 16. RGB mixing and sedimentary facies interpretation of es1x I sand formation. (a) Es_1^x I RGB mix, (b) Sedimentary facies diagram of Es_1^x I.

distribution. Low-frequency seismic data indicate a thicker reservoir, and high-frequency seismic data indicate a thinner reservoir. The single-frequency seismic data analysed in the frequency-divided data analysis process must be chosen based on the reservoir thickness. The integrated reservoir distribution can only be understood by combining the analyses of several single-frequency datasets [51]. Owing to frequent channel migration, well-developed boundary surfaces between superimposed genetic units result in a complex heterogeneous distribution of sand bodies and sedimentary phases [52]. RGB fusion technology can describe the sedimentary boundaries of sand bodies with different specific thicknesses When identifying river channels, the following three factors should be considered: special lithological sections formed between two periods of continuous and stable sedimentation by a longitudinal sedimentary sequence, distinct from the lithology of the upper and lower adjacent layers. The identification of sand bodies in different stages of river channels often involving multiple overlapping stages, which can be divided by identifying the erosion surface and the corresponding seismic wave responses of stacked sand bodies.

6. Conclusion

Using seismic sedimentology, the seismic facies characteristics of different genetic sand bodies are effectively identified, and the transformation of “seismic facies sedimentary facies” is performed. Using 90° phase volume and spectral decomposition to calibrate the lithology, the isoline of the river sand body was the most consistent with the valley waveform of the 45 Hz profile. The distribution characteristics of sand bodies at different scales can be characterised using the fusion technology of frequency-division seismic and RGB attributes.

The sediment in the Suning area comes from the Gaoyang and Shenze low uplifts in the southwest, leading to the development of

nearshore terminal fan sediments and identifying sedimentary microfacies such as distributary channels, channel overflows, floodplains, and point dams. The distributary channel sand body was the main component of the nearshore fan sand body.

By integrating the seismic RMS attributes, RGB attributes, and lithology calibration, the widespread development of distributary channel sand bodies in the Es_1^5 (SQV4–7) was found to be a favourable exploration layer. Sedimentation of distributary channels can be observed in high-frequency stratigraphic slices, where channel complexes (multiple periods of channel stacking) and wormlike reflections (abandoned channels) can be observed. The response characteristics of the distal basin microfacies were wide strips and a continuous distribution, whereas the seismic facies were mainly hill-shaped parallel sub-parallel reflections.

Data availability statement

The data that support the findings of this study are available from PetroChina Huabei Oilfield but restrictions apply to the availability of these data, whichwere use under license for the current study, and so are not publicly available. Data are however available from the authors upon reasonable request and with permission of PetroChina Huabei Oilfield.

CRediT authorship contribution statement

Xinshuai Li: Writing – review & editing, Writing – original draft, Visualization, Software, Methodology, Investigation, Conceptualization. **Qingchun Meng:** Writing – review & editing, Writing – original draft, Supervision, Resources, Project administration, Data curation. **Jun Xie:** Writing – review & editing, Writing – original draft, Visualization, Validation, Supervision, Software, Project administration, Methodology, Investigation, Conceptualization. **Xiuwei Wang:** Writing – original draft, Visualization, Validation, Software, Investigation. **Hong Chen:** Visualization, Validation, Supervision, Software. **Minmin Shao:** Writing – original draft, Visualization, Validation, Supervision, Software. **Yuzhi Zhao:** Visualization, Validation, Supervision, Software.

Declaration of competing interest

The authors declare that they have no known competing financial interests or personal relationships that could have appeared to influence the work reported in this paper.

Acknowledgements

This work was supported by the Shandong Provincial Natural Science Foundation project (ZR2022MD033).

Appendix A. Supplementary data

Supplementary data to this article can be found online at https://doi.org/10.1016/j.heliyon.2024.e26584.

References

[1] F. Jin, Z. Cui, Q. Wang, L. Li, C. Ren, M. Cui, et al., Distribution characteristics and main controlling factors of stratigraphic-lithologic reservoirs in Jizhong Depression, Lithologic Reservoirs 29 (2) (2017) 19–27, https://doi.org/10.3969/j.issn.1673-8926.2017.02.003.
[2] A. Deng, S. Zhang, F. Li, Z. Lei, Z. Huang, Q. Li, et al., Cenozoic fault activity and its control on hydrocarbon accumulation in Suning area of Raoyang sag, Bohai Bay Basin, Petroleum Geology and Recovery Efficiency 24 (3) (2017) 18–24, https://doi.org/10.13673/j.cnki.cn37-1359/te.2017.03.003.
[3] J. Zhang, Tight Reservoir Sedimentary Environment, Science Press, Beijing, 2022, pp. 184–187.
[4] A. Tomassi, F. Trippetta, R.D. Franco, R. Ruggieri, From petrophysical properties to forward-seismic modeling of facies heterogeneity in the carbonate realm (Majella Massif, central Italy), J. Petrol. Sci. Eng. 211 (2022), https://doi.org/10.1016/j.petrol.2022.110242.
[5] G. Zhong, X. Zhu, M. Matos, D. Dunlap, H. Liu, Introduction to special section: seismic sedimentology, Interpretation 6 (2) (2018), https://doi.org/10.1190/INT-2018-0314-SPSEINTRO.1. SDi-SDi.
[6] H. Zeng, What is seismic sedimentology? A tutorial, Interpretation 6 (2) (2018) https://doi.org/10.1190/INT-2017-0145.1.
[7] X. Yin, W. Huang, P. Wang, J. Wang, Q. Wang, D. Yan, et al., Sedimentary evolution of overlapped sand bodies in terrestrial faulted lacustrine basin: Insights from 3D stratigraphic forward modeling, Mar. Petrol. Geol. 86 (2017) 1431–1433, https://doi.org/10.1016/j.marpetgeo.2015.09.010.
[8] Y. Wang, F. Liu, Y. Wang, M. Zhang, Application of 3D seismic tight thin reservoir prediction and horizontal well steering technology in Sulige gas field, Oil Geophys. Prospect. 57 (S2) (2022) 87–91, https://doi.org/10.13810/j.cnki.issn.1000-7210.2022.S2.015.
[9] F.A. Alqahtani, C.A.L. Jackson, H.D. Johnson, M.R.B. Som, Controls on the geometry and evolution of humind-tropical fluvial systems: insights from 3D seismic geomorphological analysis of the Malay basin, sunda shelf, southeast asia, J. Sediment. Res. 87 (1) (2017) 17–40, https://doi.org/10.2110/jsr.2016.88.
[10] R. Riera, V. Paumard, J. Bourget, T. Allan, U. Lebrec, Evolution of the exmouth-barrow carbonate margin through the miocene: insights from 3D seismic data and field investigations (north west shelf, Australia), Sediment. Geol. 449 (2023), https://doi.org/10.1016/j.sedgeo.2023.106371.
[11] C. Ni, Mi Su, C. Yuan, H. Liu, X. Cui, Thin-interbedded reservoirs prediction based on seismic sedimentology, Petroleum Exploration and Development Online 49 (4) (2022) 851–863, https://doi.org/10.1016/S1876-3804(22)60315-X.
[12] J. Ni, D. Zhao, X. Liao, X. Li, L. Fu, R. Chen, et al., Sedimentary architecture analysis of deltaic sand bodies using sequence stratigraphy and seismic sedimentology: a case study of jurassic deposits in zhetybay oilfield, Mangeshrak Basin, Kazakhstan, Energies 15 (14) (2022), https://doi.org/10.3390/en15145306, 5306-5306.
[13] C. Williams, V. Paumard, J.M. Webster, J. Leonard, T. Salles, M. O'Leary, S. Lang, Environmental controls on the resilience of scott reefs since the miocene (north west shelf, Australia): insights from 3D seismic data, Mar. Petrol. Geol. 151 (2023) 106–108, https://doi.org/10.1016/j.marpetgeo.2023.106188.
[14] X. Zhu, Y. Dong, H. Zeng, H. Huang, Q. Liu, W. Qin, et al., A new course for the development of sedimentary geology–seismic sedimentology, J. Palaeogeogr. 21 (2) (2019) 189–201.

[15] X. Zhu, Y. Dong, H. Zeng, C. Lin, X. Zhang, Current situation and development of seismic sedimentology in China, J. Palaeogeogr. 22 (3) (2020) 397–411. Chinese Edition.
[16] C. Li, Y. Jiang, X. Fan, B. Liu, Y. Wang, J. Qi, Study on seismic sedimentology of Daqing Placanticline oilfield development, Oil Geophys. Prospect. 57 (4) (2022), https://doi.org/10.13810/j.cnki.issn.1000-7210.2022.04.019, 916-925+742-743.
[17] H. Liu, P. Wei, X. Li, Z. Hong, H. Niu, Z. Zhang, Understanding of theoretical innovation of seismic sedimentology, Lithologic Reservoir 24 (1) (2021), 7-12+19.
[18] H. Zeng, X. Zhu, R. Zhu, Q. Zhang, Seismic prediction of sandstone diagenetic facies: applied to cretaceous Qingshankou Formation in Qijia depression, Songliao Basin, Petrol. Explor. Dev. 40 (3) (2013) 266–274, https://doi.org/10.1016/S1876-3804(13)60035-X.
[19] M. Lou, H. Cai, X. He, Y. Liu, X. Huang, X. Zhang, H. Liu, Application of seismic sedimentology in characterization of fluvial-deltaic reservoirs in Xihu sag, East China Sea shelf basin, Petrol. Explor. Dev. 50 (1) (2023) 125–138, https://doi.org/10.1016/S1876-3804(22)60375-6.
[20] J. Zhang, D. Li, X. Si, Deposition and reservoir characteristics of the nearshore terminal fan of Kongdian Formation in Huimin Depression, Acta Sedimentol. Sin. 29 (1) (2011) 1–13, https://doi.org/10.14027/j.cnki.cjxb.2011.01.012.
[21] J. Zhang, C. Dai, X. Zhang, Terminal fan – a type of sedimentation ignored in China, Geol. Rev. (2) (2007) 170–179, https://doi.org/10.16509/j.georeview.2007.02.005.
[22] J. Zhang, Fluvial facies styles and their sedimentary facies models, Xinjing Pet. Geol. 40 (2) (2019) 244–252.
[23] Y. Zhao, C. Zhang, R. Zhu, W. Feng, K. Zhao, Rersearch progress of the distributive fluvial system (DFS), Pet. Geol. Oilfield Dev. Daqing 40 (6) (2021) 1–11, https://doi.org/10.19597/j.issn.1000-3754.202009042.
[24] J. Zhang, Meandering river fan facies model and its application, Geol. Rev. 68 (2) (2022) 408–430, https://doi.org/10.16509/j.georeview.2022.01.085.
[25] A. Moscariello, Alluvial fans and fluvial fans at the margins of continental sedimentary basins: geomorphic and sedimentological distinction for geo-energy exploration and development, Geological Society London Special Publications 440 (2018) 411–440, https://doi.org/10.1144/SP440.11.
[26] Y. Zhang, X. Dai, M. Wang, X. Li, The concept, characteristics and significance of fluvial fans, Petrol. Explor. Dev. 47 (5) (2020) 1014–1026, https://doi.org/10.1016/S1876-3804(20)60113-6.
[27] L. Cao, S. Chang, Y. Yao, Application of seismic sedimentology in predicating sedimentary microfacies and coalbed methane gas content, J. Nat. Gas Sci. Eng. 69 (2019), https://doi.org/10.1016/j.jngse.2019.102944.
[28] Y. Du, X. Zhu, Y. Gao, L. Li, L. Ye, X. Li, et al., Sedimentary provenance of the first member of the Shahejie Formation, lixian slope, Raoyang sag, Earth Sci. Front. 28 (1) (2021) 115–130, https://doi.org/10.13745/j.esf.sf.2020.5.12.
[29] Y. Ji, J. Du, X. Zhao, Y. Zhang, R. Zhang, Sequence stratigraphy and evolution models of the Paleogene in Raoyang sag, Jizhong depression, J. Palaeogeogr. 8 (3) (2006) 397–406.
[30] H. Zeng, X. Zhao, X. Zhu, F. Jin, Y. Dong, Y. Wang, et al., Seismic sedimentology of sub-clinoformal shallow-water meandering river delta: a case from the Suning area of Raoyang sag in Jizhong depression, Bohai Bay Basin, NE China, Petrol. Explor. Dev. 42 (5) (2015) 566–576, https://doi.org/10.1016/S1876-3804(15)30057-4.
[31] H. Dicky, E.K. Barnabas, Seismic geomorphology of the basin floor area in the Northern North Sea: evolution of the Frigg submarine channels and their influence on sediment distribution, Environ. Earth Sci. 82 (2023), https://doi.org/10.1007/S12665-023-11261-Y.
[32] B.N. Santos, C.C. Rodrigues, D.R. Franco, M. Li, M.A. Fernandes, M. Candido, et al., Integration of seismic stratigraphy and cyclostratigraphy for high resolution chronostratigraphic correlation: the Albacora Field, Campos Basin, Brazil, Mar. Petrol. Geol. 158 (PartB) (2023), https://doi.org/10.1016/J.MARPETGEO.2023.106541.
[33] T. Mukerji, A. Jørstad, P. Avseth, G. Mavko, J.R. Granli, Mapping lithofacies and pore-fluid probabilities in a North Sea reservoir: seismic inversions and statistical rock physics, Geophysics 66 (2001) 988–1001, https://doi.org/10.1190/1.1487078.
[34] A.A. Bahmani, M.A. Riahi, N. Ramin, Detection of stratigraphic traps in the Asmari Formation using seismic attributes, petrophysical logs, and geological data in an oil field in the Zagros basin, Iran, J. Petrol. Sci. Eng. 194 (2020), https://doi.org/10.1016/j.petrol.2020.107517.
[35] S. Chen, S. Cao, Y. Sun, Y. Lin, J. Gao, Seismic time-frequency analysis via time-varying filtering based empirical mode decomposition method, J. Appl. Geophys. 204 (2022), https://doi.org/10.1016/j.jappgeo.2022.104731.
[36] K. Sobczak, A.D. La Croix, J. Esterle, P. Hayes, H.G. Holl, R. Ciesiolka, et al., Geochronology and sediment provenance of the precipice sandstone and evergreen Formation in the surat basin, Australia: implications for the palaeogeography of eastern gondwana, Gondwana Res. 111 (2022) 189–208, https://doi.org/10.1016/j.gr.2022.08.003.
[37] J. Yv, H. Han, Y. Zhang, L. Cai, H. Liu, F. Lou, et al., New understanding of nearshore subaqueous fan sedimentation and re-practice of oil and gas exploration – taking the steep slope zone of Jiyang depression as an example, Acta Sedimentol. Sin. 41 (5) (2023) 1340–1353, https://doi.org/10.14027/j.issn.1000-0550.2022.138.
[38] Y. Liu, C. Liu, Y. Zhou, L. Huang, M. Bi, X. Wang, Palaeo-geomorphology restoration with double-interface seismic layer leveling: an example of Tianhuan Depression in Ordos Basin, Oil Geophys. Prospect. 54 (3) (2019) 656–666, https://doi.org/10.13810/j.cnki.issn.1000-7210.2019.03.020.
[39] W. Guo, Y. Liu, J. Zhao, X. Wang, H. Zhao, F. Ding, Deepened application of horizon-flattening technique in seismic interpretation, Oil Geophys. Prospect. 55 (5) (2020) 1110–1120, https://doi.org/10.13810/j.cnki.issn.1000-7210.2020.05.019.
[40] M. Lee, Etnyre. Finding Oil and Gas from Well Logs, Springer, New York NY, 1989, https://doi.org/10.1007/978-1-4757-5230-4.
[41] Z. Jin, X. Tan, H. Tang, A. Shen, Z. Qiao, J. Zheng, et al., Sedimentary environment and petrological features of organic-rich fine sediments in shallow water overlapping deposits: a case study of Cambrian Yuertus Formation in northwestern Tarim Basin, NW China, Petrol. Explor. Dev. 47 (6) (2020) 513–526, https://doi.org/10.1016/S1876-3804(20)60069-6.
[42] E.M. Mahon, M.W. Wallace, Sedimentology and seismic geomorphology of Paleocene coastal peatlands from the offshore Gippsland Basin, SE Australia, Sediment. Geol. 434 (2022), https://doi.org/10.1016/j.sedgeo.2022.106145.
[43] W. Wang, C. Lin, X. Zhang, C. Dong, L. Ren, J. Lin, Seismic diagenetic facies prediction of tight sandstone in the offshore sparse well area: an example from the Xihu Depression of the East China Sea Basin, J. Petrol. Sci. Eng. 216 (2022), https://doi.org/10.1016/j.petrol.2022.110825.
[44] B. Yang, L. Zhang, Z. Sun, Y. Yan, Identification and quantitative characterization of point bars in subsurface meander-river belt, taking chengdao oilfield in Bohai Bay Basin as an example, Front. Earth Sci. 10 (2022), https://doi.org/10.3389/feart.2022.932953.
[45] H. Zeng, M.M. Backus, Interpretive adventages of 90°-phase wavelets: modeling (PartII), Geophysics 70 (3) (2005) 7–34, https://doi.org/10.1190/1.1925741.
[46] A. Ulfers, C. Zeeden, B. Wagner, S. Krastel, H. Buness, T. Wonik, Borehole logging and seismic data from Lake Ohrid (North Macedonia/Albania) as a basis for age-depth modelling over the last one million years, Quat. Sci. Rev. 276 (2022), https://doi.org/10.1016/j.quascirev.2021.107295.
[47] J. Zhang, J. Gao, J. Wu, Q. Lyu, D. Fang, Sedimentary characteristics and seismic geomorphology of the upper third member of Eocene Dongying Formation in double slope systems of Laoyemiao transverse anticline, Nanpu Sag, Bohai Bay Basin, China, Mar. Petrol. Geol. 109 (6) (2019) 36–55, https://doi.org/10.1016/j.marpetgeo.2019.06.005.
[48] Y. Tang, H. Chai, H. Wang, L. Zhang, P. Chen, M. Luo, et al., Seismic geomorphology analysis and petroleum geology significance of presalt Jurassic carbonate in the right bank of Amu Darya River, Geoenergy Science and Engineering 230 (2023), https://doi.org/10.1016/j.geoen.2023.212266.
[49] D. Yue, W. Li, Y. Du, G. Hu, W. Wang, W. Wang, Z. Wang, B. Xian, Review on optimization and fusion of seismic attributes for fluvial reservoir characterization, Earth Sci. 47 (11) (2022) 3929–3943, https://doi.org/10.3799/dqkx.2022.221.
[50] S. Chang, L. Liu, Y. Cui, F. Wang, M. Song, X. Mu, Seismic sedimentary characterization of thin sand layers of shallow water deltas: a case study of Qingshuihe Formation in Fangcaohu area, Junggar Basin, Lithologic Reservoirs 34 (1) (2022) 139–147, https://doi.org/10.12108/yxyqc.20220114.
[51] D. Zhao, X. Zhu, Y. Dong, D. Wu, M. Zhu, Application of seismic sedimentology to prediction of beach and bar sandbodies in gentle slope of lacustrine basin: a case study of the Lower Cretaceous in Chepaizi area, Junggar Basin, NW China, Petrol. Explor. Dev. 41 (1) (2014) 55–61, https://doi.org/10.1016/S1876-3804(14)60006-9.
[52] M. Su, J. Liu, G. Jia, X. Du, X. Wang, W. Peng, Application of seismic frequency-division technology in delta system: a case study of the Dongying delta of the middle sub-section of the 3rd member of Shahejie formation in Dongying depression, Prog. Geophys. 29 (3) (2014) 1248–1256.